



ZnO-Ag/SiO₂ blue light blocking films prepared at relatively low temperature

Xingyang Wu¹ · Weidong Qiao¹ · Jiaqi Yu¹ · Hongdong Wang¹ · Jianhua Zhang¹

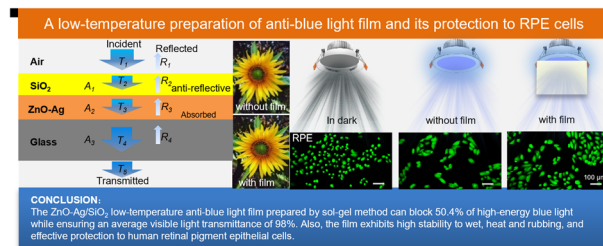
Received: 17 February 2024 / Accepted: 26 July 2024 / Published online: 14 August 2024

© The Author(s), under exclusive licence to Springer Science+Business Media, LLC, part of Springer Nature 2024

Abstract

With the increasing application of display and illumination devices, the injury of blue light to human eyes have attracted more and more attention. The current absorptive anti-blue light films require high preparation temperatures. This study prepared ZnO-Ag nanofilms by sol-gel method at relatively low temperature, 250 °C. The films were further enhanced with SiO₂ protective layer under 200 °C to improve the mechanical properties and stability, and the transmittance was investigated. The results showed that the films blocked 50.4% of blue light at wavelengths of 415–455 nm while maintained an impressive average transmittance of 98% for visible light in the range of 500–800 nm. The films had no visual effect on the display quality and the color rendering index increased only from 80.3 to 83.4, but it reduced 25% of blue light-weighted irradiance. Additionally, the films exhibited a high stability when exposed to a high temperature and humid environment (85 °C and 85% RH). Rubbing with a Teflon ball at a load of 0.5 N and a linear speed of 80 mm/min for 30 min did not show significant damage. Finally, the damage to epithelial cells exposed to blue light in the presence of the developed film was greatly alleviated.

Graphical Abstract



Keywords ZnO-Ag/SiO₂ films · Anti-blue light · Retinal pigment epithelium · Sol-gel · Plasmonic absorption

Highlight

- Relatively low temperature preparation of anti-blue light films by SiO₂-modified ZnO-doped Ag.
- Thin films with excellent optical properties without affecting the display.
- Films are stable and resistant to moisture and heat.
- Utility has been investigated through the protective effects on cells.

✉ Hongdong Wang
whd20@shu.edu.cn

¹ School of Mechatronic Engineering and Automation and Key Laboratory of Advanced Display and System Application, Ministry of Education, Shanghai University, Shanghai, China

1 Introduction

The development and wide application of display and illumination technology make people live in an increasingly blue-light-rich environment [1, 2]. Blue light, as one of the three primary colors of light, is indispensable in full-color

displays to show colorful pictures, and the screen will inevitably emit a certain amount of blue light. Studies show that continuous exposure to blue light may damage retinal pigment epithelium (RPE) cells, which can lead to visual problems such as ametropia and age-related macular degeneration [3–5]. Unfortunately, it is very difficult to avoid blue light hazards while maintaining normal display and lighting quality. Some studies show that the most destructive to RPE cells is the short-wave blue light of 415–455 nm, while the other long-wave blue light is necessary for color balance and human circadian rhythm [6, 7]. Therefore, it is necessary to mask out most of the harmful short-wave blue light and retain high transmission of the less harmful blue light to maintain normal display and lighting quality.

Reflective and absorptive coatings are two main technologies for anti-blue light. Reflective coatings are most often based on the use of two materials with different refractive indices which form a multilayer stack offering a given optical performance for blocking the specified blue light. Wang et al. prepared 14-layer blue-blocking films by ion-beam-assisted electron-beam evaporation method through nonlinear target optimization, and they found that the average transmittance of the single-sided films was lower than 3.2% at 385–415 nm, lower than 30.88% at 415–445 nm, higher than 81.9% at 445–475 nm, and higher than 95.5% at 500–800 nm [8]. Hsu et al. significantly reduced blue light transmission by stacking high refractive index of silicone and low refractive index of inorganic silicon oxide on PET using an ICPCVD system, allowing only 58.4% of blue light to transmit after stacking 6 pairs [9]. These periodically symmetric multilayer films can reflect and cut off harmful blue light and transmit other visible light. However, the overall production cost is high because these solutions require vacuum based processes and multiple layers.

Comparatively, it is unnecessary to control the thickness accurately for the absorptive anti-blue light coatings, and it is beneficial for the preparation and application of the coatings. The studies show that transparent yellow pigments as functional additives [10], and CdS, CdO, and CsPb(Cl/Br)₃ materials have good performance for masking out blue light by absorption. But organic dyes are usually less stable and prone to aging, and those inorganic materials are poisonous limiting their application [11–13]. Although nano-thick film of bismuth vanadate is stable and non-toxic and exhibits excellent performance for anti-blue light [14], the high preparation temperature of 550 °C limits the choice of substrates. Anti-blue light films should be stable and easy to be prepared with non-toxic materials at relatively low temperatures and low cost to meet more display substrates, such as polyimide whose thermal degradation is around 350 °C [15].

ZnO is stable and non-toxic, and has a band gap of 3.37 eV, and has been applied to shield ultraviolet light with very high transmittance in the visible region [16, 17]. On the other hand, the plasmon resonance absorption effect of Ag nanoparticles corresponds to the blue light band [18]. The position of the resonance peak is determined by the size, shape, and material of the nanoparticles, and more importantly, it also depends on the refractive index of the medium adjacent to the nanoparticles. Ag nanoparticles have been added to contact lenses and have been shown to filter out between 22% and 92% of blue light (400–510 nm) [19], there will be a wider range of applications for preparing anti-blue light films. Thus, the combination of ZnO and Ag (ZnO-Ag) should have great potential in shielding blue light. In this study, ZnO-Ag anti-blue light films were prepared on glass substrates by sol-gel method with different doping content of Ag nanoparticles and heating temperatures, and the transmittance was investigated. To avoid potential influence on the reflection and stability of the film, a stable low refractive index SiO₂ layer [20] was coated on the Ag-ZnO film and was also investigated.

2 Material and methods

2.1 Preparation and characterization of ZnO-Ag films

The ZnO-Ag precursor solution was prepared using zinc acetate dihydrate as the Zn source, anhydrous ethanol as the solvent, diethanolamine as the stabilizer, and AgNO₃ solution as the Ag source. Firstly, zinc acetate dihydrate was mixed with ethanol at a molar ratio of 1:50 in a brown bottle, and then diethanolamine was added at a molar ratio of 1:1 to Zn. The mixture was stirred at 30 °C for half an hour until the solution became clear. Secondly, AgNO₃ solution was added under light-proof conditions and stirred at 30 °C for 2 h at Ag/Zn molar ratios of 0.03, 0.045, 0.06 and 0.075, respectively. Finally, after aging for 24 h, the precursor solutions were obtained. ZnO-Ag films were prepared by spin coating method at 2000 r/min for 60 s under an acceleration rate of 100 r/s. The films were subsequently dried at 100 °C for 10 min and annealed at 200–400 °C for 20 min.

The UV-Vis transmittance spectra in 300–800 nm and bandgap were obtained by a HITACHI U-3900/3900H spectrophotometer at room temperature and the uncoated glass substrate was used as the reference. The surface and cross-section morphology of the films were observed by a field emission scanning electron microscope (SEM, Apreo 2C, Thermo Scientific, America). The crystalline structure of the thin films was analyzed using a Rigaku SmartLab(9KW) X-ray diffractometer (XRD) with a radiation source of Cu-K α ($\lambda = 1.54184 \text{ \AA}$). The X-ray was incident

on the sample at a grazing angle of $2\theta = 10^\circ\text{--}90^\circ$ in the θ - 2θ scan mode, with a test step angle of 0.02° . The surface chemical states of the ZnO-Ag films treated at different temperatures were examined by X-ray photoelectron spectroscopy (XPS, Quantera II from ULVAC PHI, Japan), with a monochromatic Al K α X-ray source (1486.6 eV). The X-ray spot size was set to be 650 μm and the pressure of the analysis chamber was 5.0×10^{-10} mbar. Survey scans were taken with a step size of 1.0 eV and a pass energy of 150.0 eV. High-resolution scans of Zn 2p, O 1s, and Ag 3d were taken at a pass-energy of 50.0 eV and an energy step of 0.125 eV. Prior to XPS testing, the binding energy of all elements in the thin film was calibrated using the C1s peak of carbon contamination (where the binding energy of C1s used for calibration was 284.8 eV).

As described in above, the ZnO-Ag films were prepared under relatively low temperature, and it might result in low strength and stability of the films. Thus, a SiO₂ protective coating was introduced to enhance the strength and the stability of the films. To do this, HCl was used as the catalyst for the sol-gel reaction, and anhydrous ethanol, ethyl orthosilicate (TEOS), deionized water, and concentrated hydrochloric acid were mixed in a molar ratio of 1000:250:90:2 and stirred at 40 °C for 2 h. After aging for 12 h, the mixture was spin-coated onto the ZnO-Ag films, and followed by drying and sequentially annealing at 200 °C for 30 min. The stability of the obtained films was assessed by wet heat test (85 °C, RH 85%) in a GPS-3 temperature and humidity chamber. The wear and the surface roughness were measured by MFT-5000 white light interferometer from RTEC. The friction tests were carried out with teflon balls at load of 0.5 N and linear speed of 80 mm/min for 30 min. The absolute spectrum of a white LED before and after covered with the ZnO-Ag/SiO₂ film was measured using FOREVER PCE Series Integrated Light Emission Test System (HAAS2000). Additionally, the blue light hazard and chromaticity map were measured using the OST-500 optical radiation safety test system and the SRC-600 spectral color luminance meter, respectively.

2.2 Cell experiments

Human retinal pigment epithelial cell ARPE-19 was purchased from the cell bank of the Chinese Academy of Sciences. The cells were cultured in high-sugar Dulbecco's modified Eagle medium supplemented with 10% fetal bovine serum, 100 U/mL⁻¹ penicillin, and 100 mg/mL⁻¹ streptomycin, at 37 °C in an atmosphere containing 5% of CO₂. The cells were then digested with 0.25% trypsin for blue light irradiation experiments. The cells were irradiated using a blue LED light panel with a peak wavelength of 435 nm and a half-peak width of 5 nm away from 20 cm, and the measured illuminance was 2000 lux. Three groups

of comparative experiments were carried out. They were marked by DK with the cells normally cultured in dark, BL with the cells exposed to blue light directly, and BLF with the cells exposed to blue light transmitting the filter film. The cell viability was measured by the CCK-8 method via a BioTek Epoch2 spectrophotometer, and photographs of live-dead staining and scratch assay were taken by a Nikon Ts2R fluorescent inverted microscope. The CCK-8 and live-dead staining measurements were performed after 0, 24 and 48 h of exposure, and the cell scratching was observed after 0 and 24 h of exposure.

3 Results and discussion

3.1 Structure characterization and optical performance of the ZnO-Ag films

Figure 1 shows the XRD patterns and SEM images of the ZnO-Ag films treated at different temperatures. In all the patterns, peaks at 38.14° , 44.28° , 64.42° , 77.38° , 81.52° are indexed to metallic Ag (JCPDS 04-0783), and Ag₂O and Ag₂O are not observed [21]. For the film at 200 °C, peaks can be observed at 31.78° , 56.62° , 69.14° corresponding to ZnO (100), (110), (201) planes (JCPDS No. 36-1451). In the case of those at 250 and 300 °C, new peaks at 34.42° , 36.26° , 47.56° , 56.62° , 62.86° , 66.40° , 67.96° , 69.14° correspond to ZnO (002), (101), (102), (103), (112) and (201) planes. More new peaks can be observed at 72.56° and 89.64° correspond to (200) and (203) planes. All the peaks indicate that the structure of ZnO is fibrillated zincite. And the crystallinity is getting higher as the temperature increases. The crystallite size is calculated by Debye-Scherrer formula [22], the size of ZnO is 44, 32, 30, 50, and 55 nm, and that of the crystallite size of the silver inclusions obtained via the Debye-Scherrer is 83, 59, 24, 38 and 92 nm at 200, 250, 300, 350 and 400 °C, respectively. Figure 1b–d shows the similar results as that of XRD. The films exhibit larger crystalline particles as the temperature increases.

As shown in Fig. 2a, the XPS survey spectra indicate that the films are composed of Ag, Zn, O, C and trace N. C is from contamination in the air and N is impurity residues of diethanolamine and AgNO₃. The binding energy of the peaks was referenced to C1s at 284.8 eV. Figure 2b shows the Zn2p spectrum containing two peaks at 1021.7 and 1044.8 eV with a splitting distance of 23.1 eV, indicating that the Zn element exists in the chemical state of Zn²⁺ [23, 24]. The Ag 3d spectra of the films are composed of two peaks centered at 367.1 and 373.1 eV belonging to Ag3d5/2 and Ag3d3/2, respectively. The splitting distance of the two central peaks is 6 eV, which proves the generation of metallic Ag. The two peaks have lower binding energies compared to those of bulk Ag at 368.2 and

Fig. 1 **a** XRD patterns treated at different temperatures and 100,000x SEM images of ZnO-Ag films treated at **(b)** 300, **(c)** 350, and **(d)** 400 °C

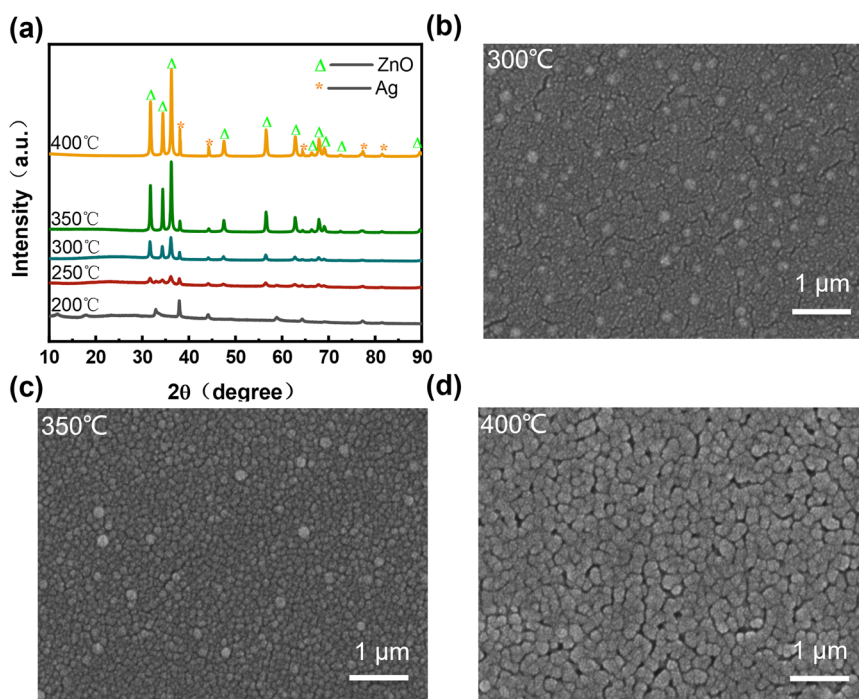
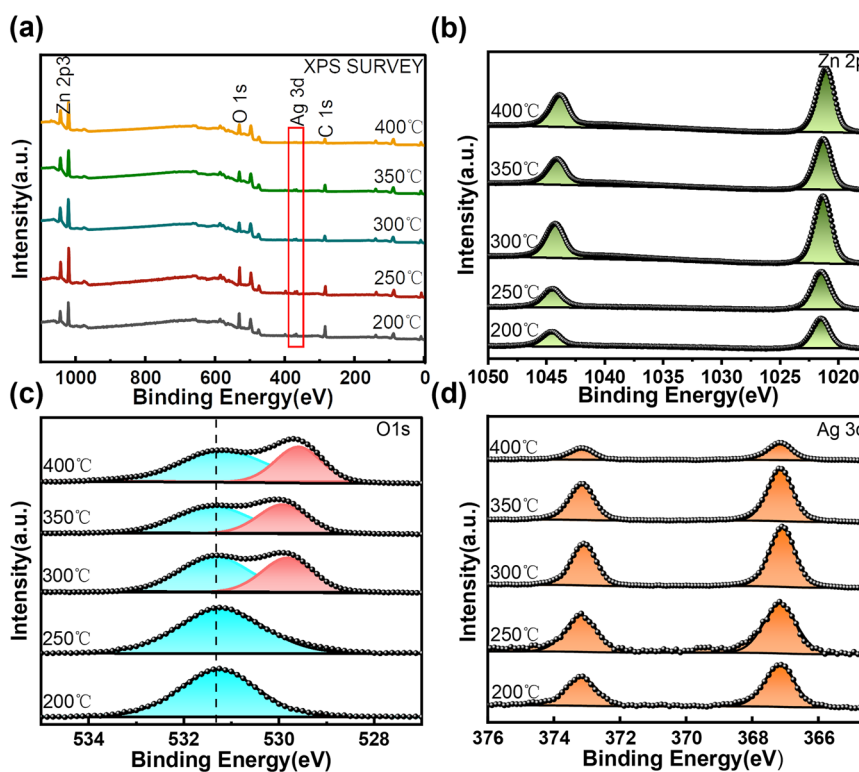


Fig. 2 **a** XPS survey spectra, **(b)** Zn 2p fractions, **(c)** O1s fractions, and **(d)** Ag 3d fractions of 6% Ag-doped ZnO-Ag films at different treat temperatures



374.2 eV. The change of the binding energy is mainly due to electron transfer from metallic Ag to ZnO [23, 24]. When metal Ag nanoparticles and ZnO nanoparticles are in contact with each other, they adjust the positions of the corresponding Fermi energy levels to the same value. As a result, many free electrons transfer to the new Fermi energy levels

of the metallic Ag nanoparticles. Since the conduction band of the ZnO nanoparticles is empty, the free electrons can tunnel into the conduction band, resulting in higher valence state of Ag [25].

The Ag/Zn atomic ratios are summarized in Table 1. The ratio decreases from 9.92% to 1.72% while the treat

temperature rises from 200 °C to 400 °C. It is clear that the amount of Ag decreases as the temperature increases. It can be considered that Ag is gradually volatilized at higher temperatures [26], which results in weakened absorption of the blue light. Two peaks at 531.4 and 529.8 eV can be observed in Fig. 2c, indicating that the oxygen exists in zinc hydroxide species or in deficient regions of ZnO and lattice oxygen of ZnO, respectively [27, 28]. As the temperature increases, the proportion of oxygen in the lattice ZnO gradually increases, which proves the continuous crystallization of ZnO. In particular, it can be seen that ZnO begins to crystallize at 250–300 °C.

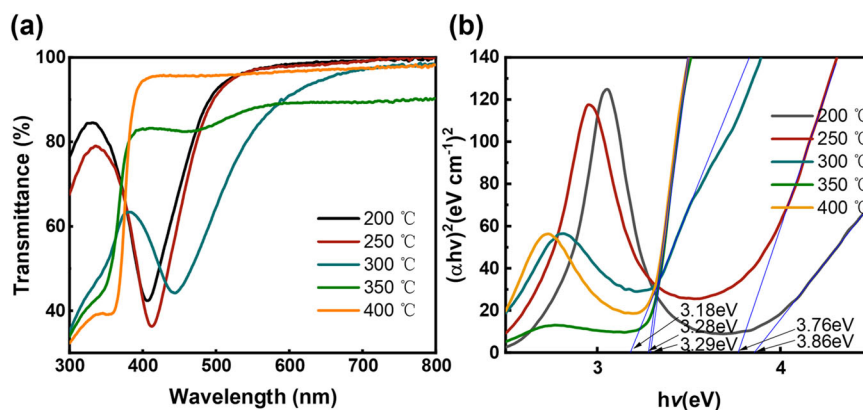
Figure 3a shows the transmittance profiles of the films doped by 6% Ag and treated at different temperatures. The films at 350 and 400 °C exhibit high transmittance to blue light and an absorption edge at 380 nm. Whereas the films at 200–300 °C show an obvious absorption peak at around 400–450 nm, and the peak red shifts with the temperature rises. The absorption edge is observed for the film at 300 °C also at 380 nm. Overall, the absorption of blue light decreases as the heat treatment temperature increases. The absorption edge may be caused by the intrinsic absorption of ZnO after continuous crystallization, which is continuously red-shifted with increasing temperature and finally stabilized near 400 nm [29]. The position of the absorption peak is between 400–450 nm, and the width of the half-peak gets larger and the absorption decreases with the temperature increase.

The bandgap (E_g) of the films was calculated from the equation $(\alpha h\nu)^{1/n} = A(h\nu - E_g)$, where α is the absorption coefficient, $\alpha = -\frac{1}{d} \ln T$, T is transmittance, d is the distance of light propagation, h is Planck's constant, A is a constant and ν is the frequency of the incident photon, for

Table 1 XPS elemental ratio analysis: Ag/Zn atomic ratio

Temperature (°C)	200	250	300	350	400
Ag/Zn atomic ratio (%)	9.92	7.17	6.02	4.82	1.72

Fig. 3 **a** Transmittance and **(b)** band gap of films doped by 6% Ag and treated at different temperatures



direct and indirect bandgap semiconductor materials, n is 1/2 and 2, respectively [30, 31]. Since ZnO is an indirect bandgap semiconductor, the value of n is 2. As shown in Fig. 1b, the bandgaps at 200 and 250 °C are 3.86 and 3.76 eV, respectively. They are significantly higher than 3.2 eV of typical ZnO. When the temperature rises to 300 °C and above, the forbidden bandwidth is around 3.2 eV as those of typical ZnO, indicating that the ZnO is gradually crystallized with the increase of temperature.

The absorption of the blue light is mainly due to the localized surface plasmon resonance (LSPR) effect of Ag [32, 33]. When the temperature increases, Ag is partially oxidized and evaporated, resulting in decrease of Ag and sequential resonance absorption, and red shift of the peak absorption position [34]. The bigger Ag nanoparticle size can also lead to red shift [19, 35]. Therefore, by changing the treat temperature, the absorption properties of the anti-blue light thin films can be adjusted.

The transmittance spectra of the films with different Ag doping concentrations at 250 °C are presented in Fig. 4a. As the Ag concentration increases, the transmittance of the films in the blue region decreases. However, the absorption peak position of the films remains relatively constant, suggesting that the Ag concentration has no significant effect on the absorption position. Furthermore, Fig. 4b illustrates that the overall band gap width slightly decreases with increasing Ag concentration, but the difference is not significant. Taking into account both the blue light blocking rate and the transmittance in the other visible light, later ZnO-Ag films were prepared by doping with 6% Ag and heat-treated at 250 °C.

3.2 The ZnO-Ag/SiO₂ films

Due to low temperature treatment, the prepared ZnO-Ag films have poor mechanical strength and stability, and are easily damaged. Here, by introducing SiO₂ protective layer, The ZnO-Ag/SiO₂ films were prepared to enhance the mechanical properties and stability of the ZnO-Ag films.

Fig. 4 **a** Transmittance and **(b)** Band gap width of the ZnO-Ag films with different Ag concentrations at 250 °C

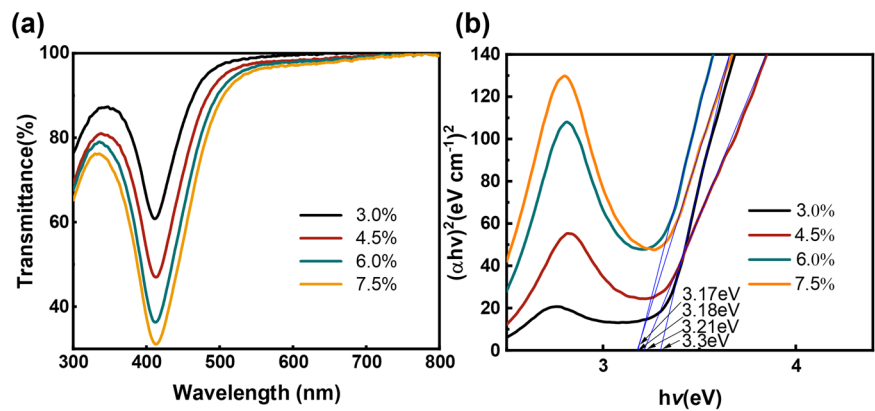


Fig. 5 **a** Transmittance of the ZnO-Ag and ZnO-Ag/SiO₂ films. **b** transmittance spectra of the ZnO-Ag/SiO₂ films after 1–7 days of wet heat treatment at 85 °C and 85% RH. And SEM images of the cross-section of the **(c)** ZnO-Ag and **(d)** ZnO-Ag/SiO₂ films

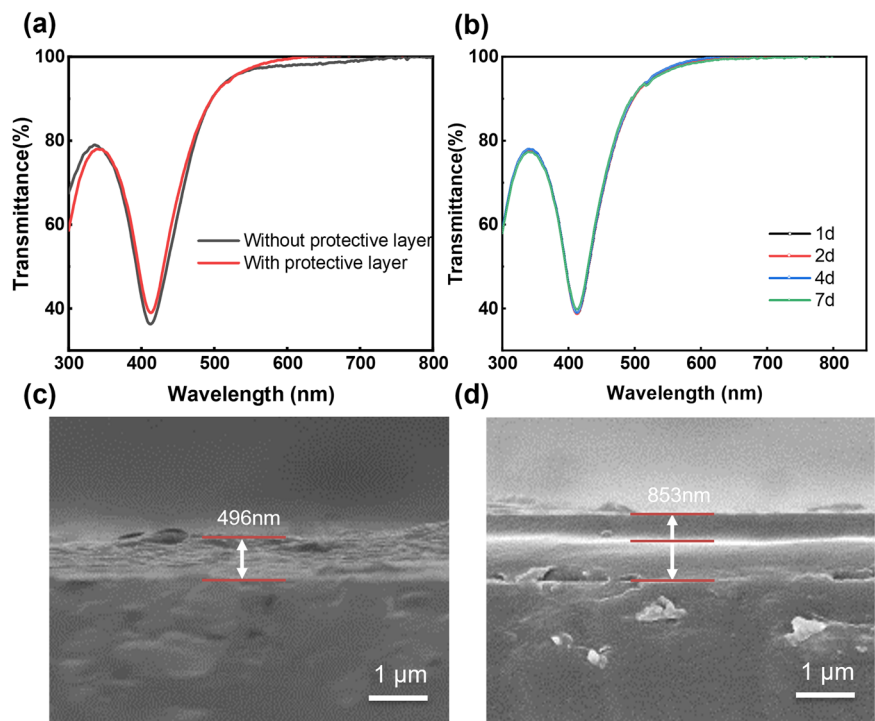


Figure 5a gives the transmittance of the ZnO-Ag and ZnO-Ag/SiO₂ films. After covered with SiO₂ layer, the average transmittance of the films increased slightly from 45.9% to 49.6% at 415–455 nm, and increased slightly from 97.1% to 98.0% at 500–800 nm. The protective layer has almost no effect on transmittance of the films. The small changes in transmittance may be attributed to the low reflective index of the SiO₂ film [20] which can increase the refractive index through the interfaces.

After 1–7 days of wet heat treatment at 85 °C and 85% RH, the color of the film without SiO₂ layer changed from yellowish to grayish purple. It is clear that the film chemically changed and lost its absorption ability to blue light. But the color of the film with SiO₂ layer remains unchanged. Figure 5b gives the transmittance spectra of the ZnO-Ag/SiO₂ films after the humid heat treatment. It

is clear that there are no any differences among these spectra. The result indicates that the films have good wet heat stability and can be used in wet heat environments. Figure 5c, d presents the SEM images of the cross-section of the ZnO-Ag and ZnO-Ag/SiO₂ films, respectively. The thickness of the ZnO-Ag film is 496 nm, and the film surface is significantly uneven. However, after introducing the SiO₂ protective layer, the thickness of the ZnO-Ag/SiO₂ film increases to 853 nm, and the film surface becomes much smooth.

Figure 6 shows the photographs and profiles of the worn surfaces on the ZnO-Ag and ZnO-Ag/SiO₂ films after rubbing with Teflon balls. The ZnO-Ag films are scratched severely with wide and deep grooves, whereas the worn scars on the ZnO-Ag/SiO₂ films are much slight and shallow. Clearly, SiO₂ layer can protect the ZnO-Ag anti-blue

Fig. 6 Photographs of the worn surfaces on the (a) ZnO-Ag and (b) ZnO-Ag/SiO₂ films and profiles on the (c) ZnO-Ag and (d) ZnO-Ag/SiO₂ films after rubbing with Teflon balls

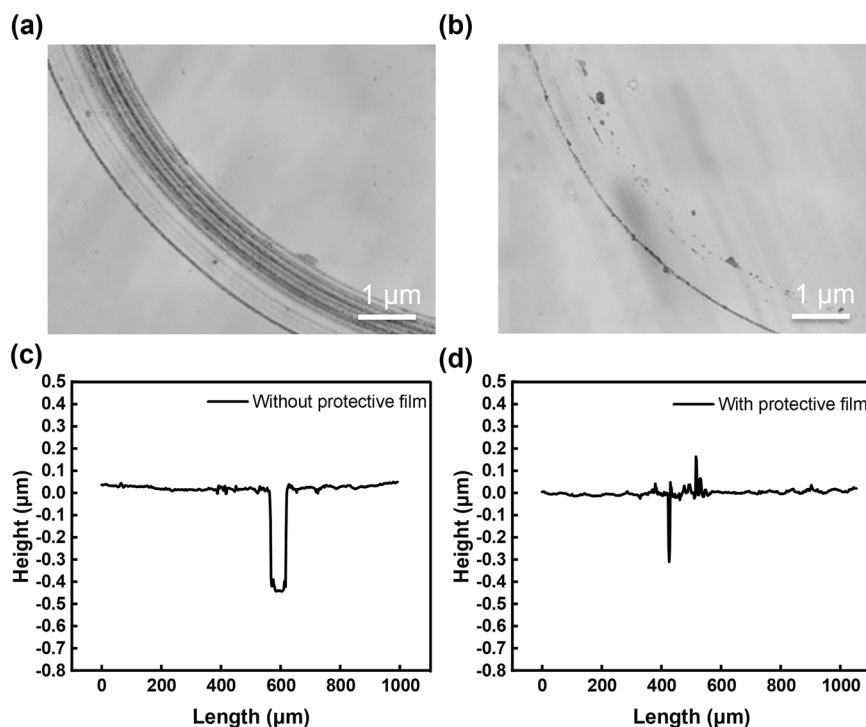
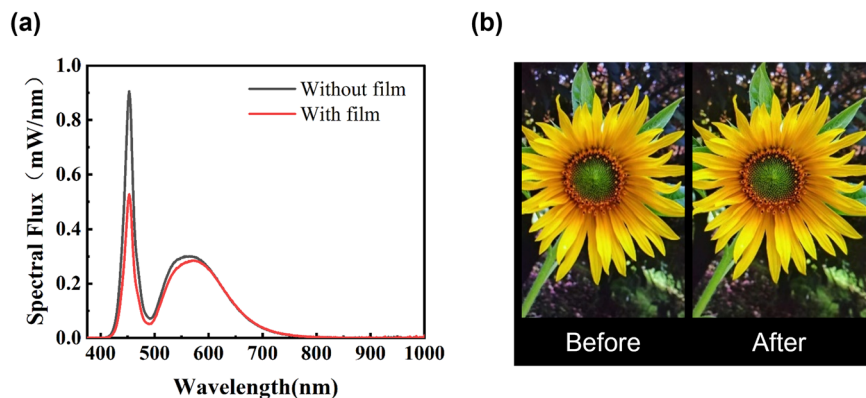


Fig. 7 Absolute spectrum (a) of a white LED and the picture on the cell phone (b) before and after covered with the ZnO-Ag/SiO₂ film



light films effectively. It is well known that acid-catalyzed SiO₂ appears in a linear form and has strong bonding, high wear resistance and strength [36].

Figure 7a presents the absolute spectra of a white LED before and after covered with the ZnO-Ag/SiO₂ film. It can be seen that after covered with the film, the intensity of blue light decreases markedly from 0.90 to 0.53 mW/nm, while that of the other visible light decreases only about 0.02 mW/nm. The blue light-weighted irradiance (L_B) decreases from 0.3212 to 0.2401 $\text{Wm}^{-2}\text{sr}^{-1}\text{nm}^{-1}$, but the color rendering index (Ra) increases from 80.3 to 83.4, suggesting that the films can ensure display quality and significantly reduce the harmful blue light. The color rendering index of the lamps is not high and the color temperature is slightly cold. After covering the film, the color temperature slightly changed to warm, resulting in an increase in the color rendering index. The color coordinate of the white LED changes from (0.3275, 0.3428) to

(0.3469, 0.3643), the change is only about 5%. Furthermore, Fig. 7b exhibits the images captured on a cell phone before and after covered with the ZnO-Ag/SiO₂ film. No changes due to covering the film can be identified, indicating that the effect of the films on the display quality is acceptable.

3.3 Protective effects of the ZnO-Ag/SiO₂ films on ARPE-19 cell against blue light

Figure 8a gives the photos of the ARPE-19 cells taken by live-dead staining method after 0, 24, and 48 h of irradiation. Over the time, little dead cells are confirmed in the DK group and most of the cells remain alive. While in the BL group, more and more dead cells are identified, live cells considerably decrease and appear blurred and deformed at the edges. In contrast, the BLF group shows only a small number of dead cells, and the dead cells considerably less

Fig. 8 **a** Photographs of ARPE-19 taken by live-dead staining method at 0, 24, 48 h and **(b)** Lateral migration assessed by the scratch assay at 0, 24 h and **(c)** Cell viability measured by CCK-8 method in DK, BL and BLF groups separately

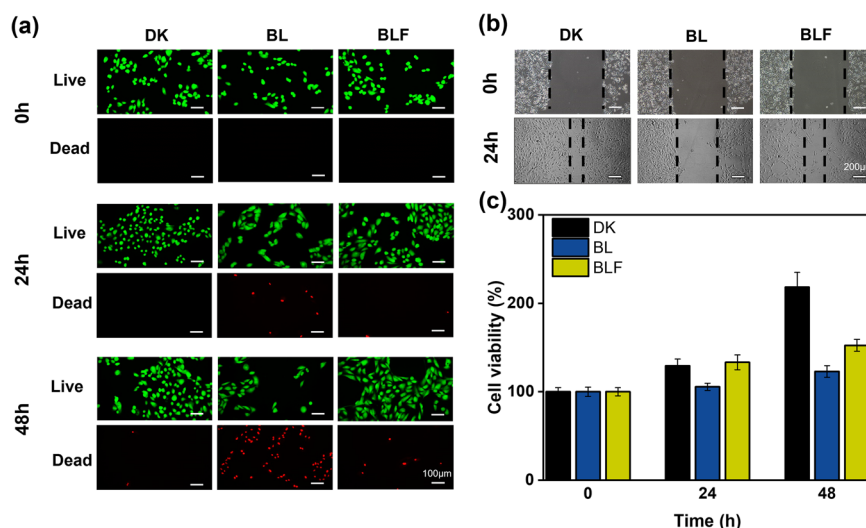


Table 2 The performance comparisons of various filters published in recent years with our results

Materials	Methods	T_{Blue}	T_{Vis}	Treat temperature	stability	Cell experiments
ZnO-Ag/SiO ₂ this work	Spin coating (double films)	49.6% (415–455 nm)	98.0% (500–800 nm)	250 °C	7d (85 °C, 85% RH)	Cell viability, migration ability
BiVO ₄ [14]	Spin coating (double films)	34.8% (415–455 nm)	85.7% (500–800 nm)	500 °C	15d (85 °C, 85% RH)	Cell viability, migration ability, mRNA expression levels
TiO ₂ , SiO ₂ [8]	14 layers	30.88% (415–455 nm)	95.5% (500–800 nm)	65 °C	not tested	not tested
Organic Si, SiO _x [9]	ICPCVD, 13 layers	58.4% (380–500 nm)	88.0%–89.0% (> 500 nm)	120 °C	not tested	not tested
ZnO/CdS [11]	Composite disks	20.0% (400–450 nm)	87.0% (> 500 nm)	140 °C	not tested	not tested
ZnO/CdO [13]	Spin coating	54.55% (400–450 nm)	91.2% (> 500 nm)	400 °C	not tested	cellular morphology
CsPb(Cl/Br) ₃ [12]	Spin coating	5.0% (459 nm)	95.0% (500–800 nm)	Room temperature	6d (UV exposure)	not tested
pigment yellow [10]	Composite disks	62.4% (400–500 nm)	81.1% (400–800 nm)	150 °C	not tested	not tested

than that observed in the BL group, despite some cells appear blurred and deformed at the edges. As Fig. 8b shows, after 24 h of cultivation, in the DK group, cell migration makes the scratch to become very shallow. But there is almost no cell migration in the BL group. And in the BLF group, the scratch width is between the DK and BL groups. These results indicate the disruption of blue light to the cells and self-healing ability of the cells, as well as the protective effect of the ZnO-Ag/SiO₂ films on cells against blue light.

Figure 8c presents the cell viability of the CCK-8 experiments, where the cell viability of the three groups

were set to 100% at initial state. After 24 h, the change in the cell viability of the BL group can be ignored, while the cell viability of the DK and BLF groups increases significantly. After 48 h, the cell viability of the DK group shows the highest value. Although both the BL and BLF groups exhibit an increase in the cell viability, the cell viability of the BLF group is much higher than that of the BL group. Clearly, blue light has an inhibitory effect on cell reproduction, and the ZnO-Ag/SiO₂ films possess protective effect on ARPE-19 cells. Table 2 shows the performance comparison of this work to various anti-blue light films published in recent years.

4 Conclusions

This work prepared ZnO-Ag anti-blue light films using sol-gel method at low temperature and were further coated with a protective SiO₂ layer with HCl as the catalyst. The transmittance investigation results showed that the obtained ZnO-Ag/SiO₂ films blocked 50.4% of short-wave blue light at 415–455 nm, and maintained an average transmission of 98% in the other visible light of 500–800 nm. The films had little effect on color coordinate and actual display. The transmittance did not change even after 7 days of heat wet treatment.

After covered the blue light with the ZnO-Ag/SiO₂ films, the ARPE-19 cells exhibited much higher cell viability compared with those without the films. In addition, the films also showed high friction resistance.

Acknowledgements This work was financially supported by the National Natural Science Foundation of China (52275203) and the Tribology Science Fund of the State Key Laboratory of Tribology (SKLTKF20A01).

Author contributions XW: Investigation, Writing—Review & Editing. WQ: Investigation, Methodology, Writing—Original draft preparation. JY: Validation, Formal Analysis. HW: Funding Acquisition, Methodology, Supervision. JZ: Resources, Conceptualization.

Compliance with ethical standards

Conflict of interest The authors declare no competing interests.

References

- Kimura N, Sakuma K, Hirafune S et al. (2007) Extrahigh color rendering white light-emitting diode lamps using oxynitride and nitride phosphors excited by blue light-emitting diode. *Appl Phys Lett* 90:51109
- Wang C, Takeda T, Ten Kate OM et al. (2017) Ce-doped La₃Si_{6.5}Al_{1.5}N_{9.5}O_{5.5}, a rare highly efficient blue-emitting phosphor at short wavelength toward high color rendering white LED application. *ACS Appl Mater Interfaces* 9:22665–22675
- Algvere PV, Marshall J, Seregard S (2006) Age-related maculopathy and the impact of blue light hazard. *Acta Ophthalmol Scand* 84:4–15
- Dai X, Tang Z, Ju Y et al. (2021) Effects of blue light-exposed retinal pigment epithelial cells on the process of ametropia. *Biochem Biophys Res Co* 549:14–20
- Yang PM, Cheng KC, Yuan SH, Wung BS (2020) Carbon monoxide-releasing molecules protect against blue light exposure and inflammation in retinal pigment epithelial cells. *Int J Mol Med* 46:1096–1106
- Arnault E, Barrau C, Nanteau C et al. (2013) Phototoxic action spectrum on a retinal pigment epithelium model of age-related macular degeneration exposed to sunlight normalized conditions. *PLoS ONE* 8:e71398
- Ishizawa M, Uchiyumi T, Takahata M, Yamaki M, Sato T (2021) Effects of pre-bedtime blue-light exposure on ratio of deep sleep in healthy young men. *Sleep Med* 84:303–307
- Wang Y, Zhou X, Li Q et al. (2021) Blue-blocking optical thin films with controllable cutoff slope. *Chin Opt* 14:544–551
- Hsu C, Liu T, Hsieh I, Han P, Lien S (2016) Blue-light shielding, hard and hydrophobic inorganic and organic silicon stack-films prepared on flexible substrates. *Thin Solid Films* 618:146–150
- Su K, Tao Y, Zhang J (2021) Highly transparent plasticized PVC composite film with ideal ultraviolet/high-energy short-wavelength blue light shielding. *J Mater Sci* 56:17353–17367
- Han C, Wang F, Gao C et al. (2015) Transparent epoxy-ZnO/CdS nanocomposites with tunable UV and blue light-shielding capabilities. *J Mater Chem C* 3:5065–5072
- Huang G, Huang Y, Xu W et al. (2019) Cesium lead halide perovskite nanocrystals for ultraviolet and blue light blocking. *Chin Chem Lett* 30:1021–1023
- Yang Y, Li Y, Yin L, Chen L, Zhang J (2018) Low cost ZnO/CdO thin films effectively reduce blue light-induced damage to RPE cells by display and lighting devices. *Mol Cryst Liq Cryst* 676:72–82
- Yang Y, Ju Y, Li Y et al. (2020) Transparent nanostructured BiVO₄ double films with blue light shielding capabilities to prevent damage to ARPE-19 cells. *ACS Appl Mater Inter* 12:20797–20805
- Bretos I, Jiménez R, Ricote J, Calzada ML (2018) Low-temperature crystallization of solution-derived metal oxide thin films assisted by chemical processes. *Chem Soc Rev* 47:291–308
- Özgür Ü, Alivov YI, Liu C et al. (2005) A comprehensive review of ZnO materials and devices. *J Appl Phys* 98:41301
- Wang L, Zhang X, Li B et al. (2011) Superhydrophobic and ultraviolet-blocking cotton textiles. *ACS Appl Mater Inter* 3:1277–1281
- Liu S, Chen G, Prasad PN, Swihart MT (2011) Synthesis of monodisperse Au, Ag, and Au–Ag alloy nanoparticles with tunable size and surface plasmon resonance frequency. *Chem Mater* 23:4098–4101
- Elsherif M, Salih AE, Alam F et al. (2024) Plasmonic contact lenses based on silver nanoparticles for blue light protection. *ACS Appl Nano Mater* 7:5956–5966
- Gerancheva OE, Pashkina YO, Rusanova TY, Bondareva LN (2018) Sol-gel synthesis of anti-reflective mesoporous coatings based on silicon dioxide. *Glass Ceram+* 74:428–431
- Waterhouse GIN, Bowmaker GA, Metson JB (2001) The thermal decomposition of silver (I, III) oxide: a combined XRD, FT-IR and Raman spectroscopic study. *Phys Chem Chem Phys* 3:3838–3845
- Jeffery GA (1957) Elements of x-ray diffraction (Cullity, B. D.). *J Chem Educ* 34:A178
- Chen C, Zheng Y, Zhan Y et al. (2011) Enhanced Raman scattering and photocatalytic activity of Ag/ZnO heterojunction nanocrystals. *Dalton Trans* 40:9566–9570
- Shi H, Chen J, Li G et al. (2013) Synthesis and characterization of novel plasmonic Ag/Ag_x-CNTs (X = Cl, Br, I) nanocomposite photocatalysts and synergetic degradation of organic pollutant under visible light. *ACS Appl Mater Inter* 5:6959–6967
- Liang YM, Guo N et al. (2016) Facile synthesis of Ag/ZnO microflowers and their improved ultraviolet and visible light photocatalytic activity. *New J Chem* 40:1587–1594
- Jiang CZ, Fan XJ, In-situ TEM (2000) observation of silver nanocrystals in an Ag-implanted SiO₂ film. *Surf Coat Technol* 131:330–333
- Lv J, Zhu Q, Zeng Z et al. (2017) Enhanced photocurrent and photocatalytic properties of porous ZnO thin film by Ag nanoparticles. *J Phys Chem Solids* 111:104–109
- Tao J, Gong Z, Yao G et al. (2016) Hydrothermal growth of nanorod arrays and in situ conversion to nanotube arrays for highly efficient Ag-sensitized photocatalyst. *J Alloys Compd* 689:451–459
- Moulder JF, Chastain J, King RC (1992) Handbook of x-ray photoelectron spectroscopy : a reference book of standard spectra for identification and interpretation of XPS data. *Chemical Phys Lett* 220:7–10

30. Li C, Zhang D, Han S et al. (2003) Diameter-controlled growth of single-crystalline In_2O_3 nanowires and their electronic properties. *Adv Mater* 15:143–146
31. Liu J, Liu Y, Liu N et al. (2015) Metal-free efficient photocatalyst for stable visible water splitting via a two-electron pathway. *Science* 347:970–974
32. Homola J (2006) Electromagnetic theory of surface plasmons. In: Homola J (ed) *Surface plasmon resonance based sensors*. Springer Berlin Heidelberg, Berlin, Heidelberg, p 3–44
33. Xia Y, Halas NJ (2005) Shape-controlled synthesis and surface plasmonic properties of metallic nanostructures. *MRS Bull* 30:338–348
34. Pivin JC, García MA, Hofmeister H et al. (2002) Optical properties of silver clusters formed by ion irradiation. *Eur Phys J D At Mol, Opt Plasma Phys* 20:251–260
35. Olson J, Dominguez-Medina S, Hoggard A et al. (2015) Optical characterization of single plasmonic nanoparticles. *Chem Soc Rev* 44:40–57
36. Peng K, Chen E, Zhou LP, Zhu JJ, Li DY (2014) Effects of catalyst on the transmittance and stability of SiO_2 antireflective film prepared by sol-gel method. *Adv Mater Res* 834-836:462–465

Publisher's note Springer Nature remains neutral with regard to jurisdictional claims in published maps and institutional affiliations.

Springer Nature or its licensor (e.g. a society or other partner) holds exclusive rights to this article under a publishing agreement with the author(s) or other rightsholder(s); author self-archiving of the accepted manuscript version of this article is solely governed by the terms of such publishing agreement and applicable law.